This is a repository copy of *Automated Piecewise Linear Regression for Analyzing Structural Health Monitoring Data*.

White Rose Research Online URL for this paper:
https://eprints.whiterose.ac.uk/213913/

Version: Accepted Version

Title No. 121-M18

Automated Piecewise Linear Regression for Analyzing Structural Health Monitoring Data

by H. Garg, K. Yang, A. G. Cohn, D. Borman, S. V. Nanukuttan, and P. A. M. Basheer

The recent increased interest in structural health monitoring (SHM) related to material performance has necessitated the application of advanced data analysis techniques for interpreting the real-time data in decision-making. Currently, an accurate and efficient approach for the timely analyses of large volumes of uncertain sensor data is not well-established. This paper proposes an automated clustering-based piecewise linear regression (ACPLR)-SHM methodology for handling, smoothing, and processing large data sets. It comprises two main stages, where the gaussian weighted moving average (GWMA) filter is used to smooth noisy data obtained from electrical resistance sensors, and piecewise linear regression (PLR) predicts material properties for assessing the performance of concrete in service. The obtained values of stabilized resistance and derived values of diffusion coefficients using this methodology have clearly demonstrated the benefit of applying ACPLR to the sensor data, thereby classifying the performance of different types of concrete in service environments.

INTRODUCTION

The extensive demand for a reliable estimation of the material performance during the service life of structures, along with the prediction of their current and future conditions in the service environment, has expedited innovations in structural health monitoring (SHM) systems (McCarter et al. 2012; Frangopol and Kim 2014). They use the data obtained from the specifically designed sensors and sensing technologies installed in a structure to continuously monitor either the changes in materials or structural characteristics of members, thereby assessing the structure's performance in service. They notify any defects in the structure so that necessary remedial and timely repairs can be carried out and perform real-time maintenance, with the ultimate objective of ensuring the structure's safety and serviceability (Farrar and Worden 2012).

SHM is generally used for two purposes. First, SHM can be used to monitor the changes in structural behavior or conditions of the structure such as acceleration, displacement, or rotation that would indicate the integrity and structural damage and assess the performance of the structure during its service life (Brownjohn et al. 2011; Dong and Catbas 2021). Second, SHM can be used to identify physical and/or chemical changes in material properties caused by the interaction between the material in structural members and the exposure environment, including corrosion of the embedded steel in reinforced concrete members, delamination or cracking, and void formation, all of which affect

the performance of the whole structure (Bungey et al. 2006; ACI Committee 444 2021). Thus, an accurate diagnosis of the structural behavior or material properties from the SHM data can be used for decision-making processes, including cost-effective repair and maintenance strategies.

With recent developments in both types of monitoring strategies, the installation of multiple sensors for long-term monitoring of structures normally generates a huge amount of complex, uncertain sensor data (Smarsly et al. 2016). Hence, data handling, smoothing, and analyzing large amounts of sensor data from structures to properly decide on structural repair and maintenance is currently a challenge (Nanukuttan et al. 2017a; Yavuz and Safak 2019). In addition, a wrong diagnosis due to inaccurate data analysis may trigger untimely maintenance or repair, resulting in an increased cost of maintenance (Chandrasekaran 2019) or premature failure. These concerns have led to the implementation of advanced computational techniques, such as artificial intelligence (AI) algorithms, for analyzing the SHM data, thereby resolving any issues related to data processing and decision-making.

The rising trend of the application of AI algorithms in SHM has the potential to revolutionize the concrete industry (Ahmed et al. 2019). AI uses machine learning (ML) algorithms such as those based on statistics, probability, and neural networks to train models and provides a way to access massive amounts of information, process it, analyze it, and implement solutions to various problems (Pan and Zhang 2021; Flah et al. 2021).

RESEARCH SIGNIFICANCE

A review of the literature highlighted that considerable research has been undertaken in the field of analyzing SHM data using ML algorithms to capture changes in natural vibration frequencies, mode shape, modal strain energy, dynamic flexibility, and strain measurements (Yu et al. 2011; Karbassi et al. 2014; Aydin and Kisi 2015; Diez et al. 2016). However, an accurate and efficient approach for the timely analysis of large volumes of noisy and uncertain data to capture material properties is not well established. Therefore, this paper explicitly focuses on SHM undertaken for assessing changes in material performance and thus proposes an automated AI-based SHM methodology to effectively extract

and interpret knowledge on changes in material properties obtained from SHM data for predicting the in-service performance of concrete structures.

SENSING METHODOLOGIES FOR ASSESSING CONCRETE PERFORMANCE IN SERVICE

SHM is used to assess the material characteristics of structures and thereby determine their current condition and predict the in-service performance of the structure (Dong and Catbas 2021). Degradation mechanisms such as chloride ion ingress, carbonation, corrosion of steel reinforcement, freezing-and-thawing damage, and alkali-aggregate reaction are some of the principal causes affecting the performance of materials in structures (Bungey et al. 2006; ACI Committee 201 2016). Researchers and practitioners have developed and used many sensors and sensing technologies to identify and measure changes in materials that may have an adverse effect on the future performance of structures. A list of various sensors or sensing techniques used to assess changes in material properties is provided in Table 1. These sensors measure the physical changes in the concrete due to environmental and loading conditions, as well as monitor the ambient environmental conditions where the material is exposed. Among the sensors listed in Table 1, the electrical resistance sensor is one of the most reliable types of sensors for use in concrete structures.

Electrical resistance monitoring

It is known that electrical resistance is a property that can be used to analyze early-age variations in cement hydration, the effect of temperature and moisture content, ingress of chloride ions that could induce corrosion of the embedded reinforcing steel, carbonation, and performance of material with time (Basheer et al. 2002; Nokken and Hooton 2007; Nanukuttan et al. 2017b). As diffusion and permeability are the primary mechanisms of transporting chloride ions or carbon dioxide in the concrete, these parameters cannot be monitored regularly but can be measured intermittently (Garboczi and Bentz 1992; Nanukuttan et al. 2015). On the other hand, the rate of corrosion can be monitored. Still, as this data is obtained after the initiation of corrosion, it is ineffective for carrying out preventative maintenance. However, these parameters are related to electrical resistance; thus, they can be determined from the steady-state resistance values for predicting the performance of concrete. However, electrical resistance is also affected by ambient environmental conditions and changes in the hydration of cement, and, as a result, interpretation becomes difficult due to these variations in most of the measurements.

Therefore, the focus of this paper is to demonstrate the methodology to smooth noisy and uncertain electrical resistance sensor data and analyze it using an automated clustering-based automated piecewise linear regression (ACPLR). The steady-state resistance values obtained are used to determine the diffusion coefficient values for assessing the performance of concrete for prognosis.

EXPERIMENTAL PROCEDURE

Materials, concrete mixtures, and site conditions

The study used three high-performance concrete mixtures manufactured with portland cement (PC), pulverized fuel ash (PFA), and microsilica (MS), as reported in Table 2. The experiment used CEM-I cement, 10 and 20 mm size crushed basalt as the coarse aggregate (CA), and medium-graded natural sand as the fine aggregate (FA). A polycarboxylic acid-based polymer was used as a high-range water-reducing admixture (HRWRA) that was added to the mixtures to ensure the consistency of the mixture was satisfactory while the water-binder ratio (w/b) remained at 0.3 (Yang et al. 2014).

Two concrete blocks of dimensions 410 x 100 x 250 mm were cast for each mixture and were cured in a constant-temperature water tank (20 ± 2°C) for 3 days. These blocks were kept at a constant room temperature (20 ± 1°C) for 90 days before relocating them to an open area 1 m from a three-story building (Latitude 54° 39' N, Longitude 6° 12' W). The two 410 x 250 mm sides were exposed, and the remaining sides were sealed with two coats of epoxy-based paint to ensure a uniaxial moisture movement. The exposed side of the specimen was placed vertically to let rain flow freely on the surface (Yang et al. 2014). Further details on materials, preparation of specimens and testing were detailed by Yang et al. (2014).

Sensors and monitoring

The concrete blocks were embedded with a multielectrode array within the cover zone of specimens for acquiring electrical resistance and temperature. A resistance meter was used to measure the electrical resistance between the electrode pairs (stainless steel pins, Fig. 1(a)) at three depths: 15, 25, and 45 mm from the surface of the blocks. Three thermistors were also embedded at 15, 25, and 45 mm depths to measure changes in temperature in the concrete cover zone. The monitoring started after 3 days of curing, and the data were recorded using a portable data logging system (Fig. 1(b)) for 6 months. The data were captured at a 10-minute frequency for a period of 172 days, and over 24,000 sets of data were reported in the study.

As-measured resistance measurements inside concrete specimens

The average as-measured resistance data for the two concrete blocks at 15 mm depth from the concrete surface for the three concrete mixtures are shown in Fig. 2. It can be seen that, overall, the resistance increased over the period for the three concrete mixtures. In comparison, the rate of increase in resistance in MS was the fastest, rising from 10 to 190 kΩ, followed by PC and PFA, rising from 5 to 30 kΩ in 6 months. It can be observed that concrete blocks were sensitive to the natural environment. After exposing them to the natural condition (day 90), there were substantial diurnal variations in the data set, especially for the MS blocks. No major difference can be seen between PFA and PC. However, it can be observed that the resistance of PFA rose steadily, while PC can be seen as stable after 100 days. The 6-month data shown in Fig. 2 depicts that the presence of a

Table 1—Types of sensors used for assessing material performance

Sensors	Measurands	Purpose	Limitations
Corrosion sensors, electrical resistance probes, half-cell potential	Corrosion (Perveen et al. 2014)	Used to monitor corrosion rate in structure due to changes in concrete chemical environment.	These are not recommended to monitor corrosion with epoxy-coated reinforcing bars, as this creates barrier between metals and alters results.
Electrical resistance sensors, chloride ion sensors	Chloride content (Montemor et al. 2006)	Used to detect presence of chemicals such as chloride ions in reinforced concrete (RC) structures to prevent premature corrosion.	They are only used for local measurement; hence, prior knowledge of likely locations where chloride values could increase is needed for positioning sensors.
Humidity sensor, weather station, fiber Bragg grating (FBG) sensors	Humidity (Tanner 1990; Zhang et al. 2010)	Used to measure relative humidity (RH) in concrete and determine moisture content in and around the concrete.	They are sensitive to thermal and environmental conditions and may result in wrong measurements.
Load cell, weigh-in-motion sensors	Load (Hernandez 2006; Ballo et al. 2014)	Used to measure deformations caused due to external force applied to structure.	They are bulky and require expensive electronic devices along with them.
pH sensors, fiber-optic sensor (FOS)	pH (Basheer et al. 2004)	Used to measure pH values of the concrete, which determines level of acidic or basic nature.	FOS are currently not suitable for long-term monitoring of pH and require careful handling.
Piezometers	Pressure (Kalkani 1992)	Used to measure changes in water table or pore water pressure.	They are sensitive to temperature and moisture conditions.
Temperature sensors, thermistors, FOS, thermocouples	Temperature (Rai 2007)	Used to monitor temperature changes in concrete structure due to hydration and pore structure changes.	Self-heating in sensor may cause errors in measurement. No linear relationship between the two variables.
Weather station, rain gauges	Precipitation (Fabo et al. 2020)	Used to measure precipitation.	They are only used to measure ambient environmental conditions.

Table 2—Mixture proportions and compressive strength of concretes

| Types of concrete | Proportions of binder material, % by mass | Material quantities, kg/m^3 | | | | | | w/b | HRWRA | Compressive strength, N/mm^2 | |
		PC	PFA	MS	Water	FA	CA			28 days	56 days
PC	100% PC	485	0	0	145	689	1150	0.3	1.3	81.8	87.3
PFA	80:20 PC:PFA	388	97	0	145	689	1150	0.3	1.4	81.3	90.7
MS	73:7:20 PC:MS:PFA	352	97	36	145	689	1150	0.3	1.5	84.2	94.6
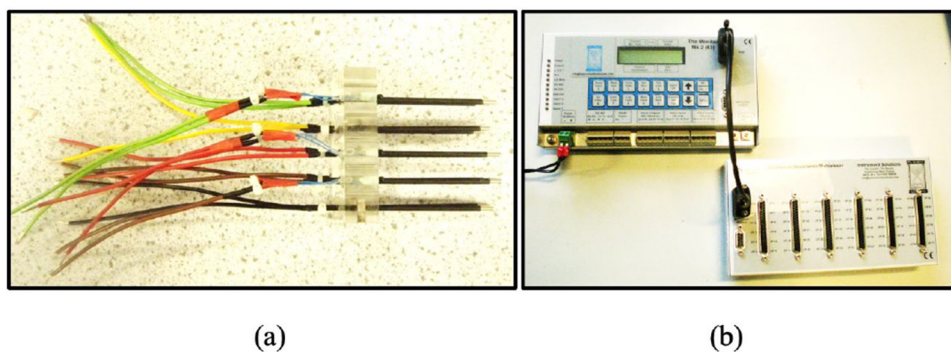
Fig. 1—(a) Sensor block used for embedding in specimen; and (b) monitoring system.

large amount of uncertain data meant there are challenges that require handling, smoothing, and processing SHM data to identify the standard steady-state resistance values of the three mixtures for decision-making. Thus, the authors aim to use all the available data sets and present an AI-based SHM methodology to handle, smoothen, and analyze the electrical resistance data.

METHODOLOGY USED FOR AI-BASED SHM DATA ANALYSIS

In this section, an AI-based SHM methodology is presented to smooth noisy data obtained from the electrical resistance sensors and analyze it to predict the performance of the concretes. The workflow of the AI-based SHM methodology is illustrated in Fig. 3, followed by a detailed analysis in later sections.

Fig. 2—Average as-measured resistance data at 15 mm depth for three mixtures.
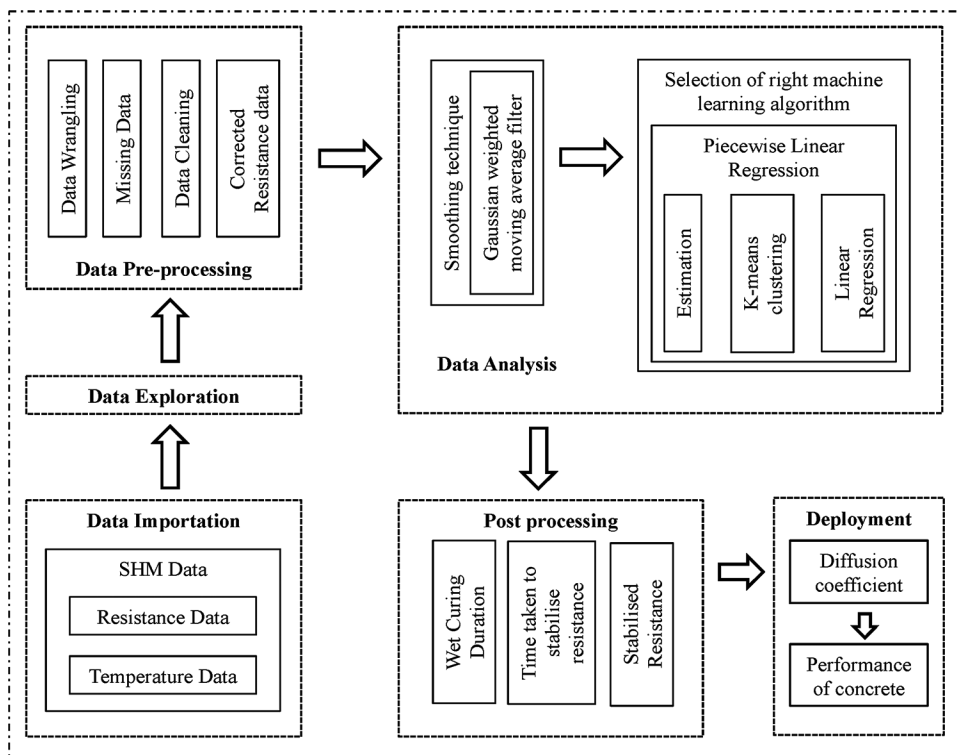
Fig. 3—Methodology used to clean, analyze, and process SHM data.
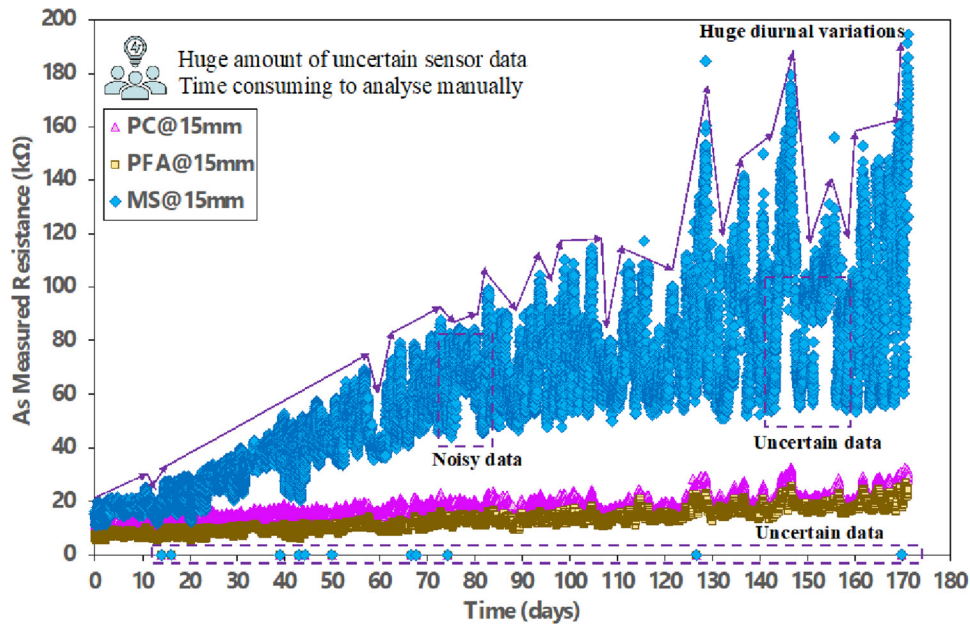
Data preprocessing

The measurements from the thermistors were converted to temperature (°C) using the Steinhart-Hart equation (Steinhart and Hart 1968)

$$T = 1/[A + B \ln R + C (\ln R)^3] - 273.1 \qquad (1)$$

where T is the temperature in °C; R is the measured resistance in ohms (Ω); ln is the natural logarithm; and A, B, and C are coefficients, $1.28 \times 10^{-3}\,K^{-1}$, $2.36 \times 10^{-4}\,K^{-1}$, and $9.31 \times 10^{-8}\,K^{-1}$, respectively, based on the type of thermistor used.

The data set thus obtained was re-examined, and it was observed that there were missing values, duplication of data, and invalid data, presumably due to sensor connection issues while moving the specimens from one place to another after 90 days. These points were identified and eliminated from the data to reduce their influence on the analysis and to improve the signal-to-noise ratio. Further, the temperature variations were very high for the data captured every 10 minutes, and hence, daily average diurnal variations were considered for further data analysis.

Correction of resistance data for temperature variations

The measured electrical resistance is affected by the changes in temperature and moisture content of the concrete (McCarter et al. 2005; Nanukuttan et al. 2017a; Demircili-ioğlu et al. 2019). The effect of variations in temperature on the measured electrical resistance could be removed by expressing the resistance at a reference temperature—say, 25°C. For this, an Arrhenius relationship (Eq. (2)) was used (McCarter et al. 2012)

$$\rho_x = \rho_y e E_a / R_g [1/T_{k,x} - 1/T_{k,y}] \qquad (2)$$

where ρ_y is the resistance (kΩ) recorded at the temperature at $T_{k,x}$ (K) is used to obtain equivalent resistance ρ_x at reference temperature ($T_{k,y}$); R_g is the universal gas constant (8.3141 × 10^{-3} kJ/mole/K); and E_a is the activation energy (kJ/mol). As both ρ_x and ρ_y have the same geometrical factors, resistivity was replaced by resistance for the analysis (Nanukuttan et al. 2017a).

The activation energy was determined by following the procedure suggested by McCarter et al. (2012), as described herein. The values of E_a/R_g for all concrete mixtures can be determined from Eq. (3). The equation linearizes the data by plotting the natural log of resistance (ρ) against $1000/T$, and the slope thus obtained is E_a/R_g with ρ_0 as pre-exponential constant (kΩ). E_a at each electrode pair for concrete can then be calculated by multiplying the slope with the value of R_g, which, when substituted in Eq. (3), would remove the temperature effects from the field measurements (McCarter et al. 2012)

$$\ln \rho = \ln \rho_0 + \frac{E_a}{R_g T} \qquad (3)$$

McCarter et al. (2012) depicted a linear relationship from the equation by plotting every 15th set of data points from 1 to 150 days. Nanukuttan et al. (2017a) plotted all data obtained from the measurement period and observed that there were multiple parallel lines and for each line, the value R^2 was similar. Thus, it was suggested that one of these lines could be used to determine the activation energy. However, for the data reported in this paper, when all the available data were plotted, a significant scatter of data during the initial 45 days was observed for both PFA and MS concretes, indicating no clear relationship, which was not observed for the PC concrete (Fig. 4). The slope values obtained using all the data for PFA and MS were three times higher than that determined by McCarter et al. (2012) and Nanukuttan et al. (2017a). However, after 45 days, a linear relationship was obtained for both these concretes, giving similar results to those reported by McCarter et al. (2012). This is potentially the case because the total cementitious material content and the reactivity of SiO_2, CaO, Al_2O_3, and Fe_2O_3 might have influenced the rate of hydration and, hence, the total heat generated at an early age (Nehdi and Soliman 2011; Jansen et al. 2012; Schöler et al. 2017).

Up to approximately 50% hydration of PC is completed within 1 day of adding water to the cement, 80% within 28 days, and the remaining hydration gradually occurs within the next 3 to 4 months. At this stage, the hydrated portland cement paste is considered to have reached a stable state (Scrivener and Nonat 2011). On adding supplementary cementitious materials (SCMs), the pozzolanic reaction normally starts after 3 days of the hydration of portland cement and continues beyond 28 days, depending on the type of SCM, curing condition, and proportion of the binder materials (Zelić et al. 2000). Therefore, for further analysis, the matured concrete data after 45 days were considered for
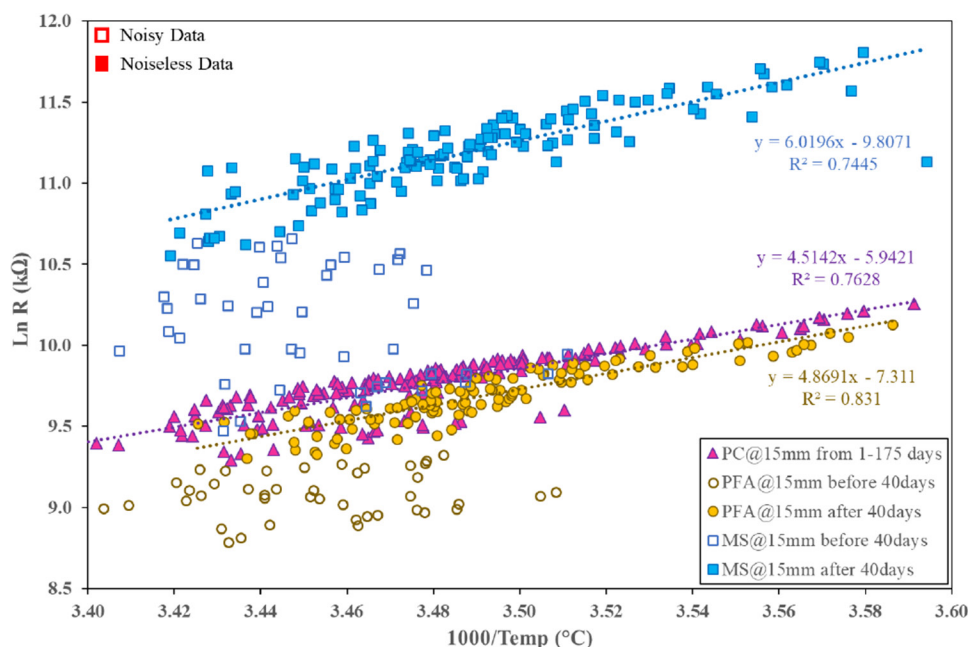
Fig. 4—Removal of noise from 25 mm depth data for establishing Arrhenius equation for PC, PFA, and MS. (Note: Noisy data presented herein for PFA and MS are from first 45 days of reaction; thereafter, trend becomes linear, whereas noise is absent for PC.)

estimating the activation energy and reducing the effect of cement hydration and pozzolanic reactions on the calculated activation energy.

When the activation energy was estimated using the aforementioned procedure, it is interesting to note that the graph now depicts a linear correlation, as shown in Fig. 4. The estimated activation energy, E_a, for each electrode pair for all concrete mixtures of each sample from Eq. (3) is reported in Table 3. It shows that not much variation is seen in PC and PFA and lies within the range of 35 to 47, while MS lies in the 50 to 57 kJ/M range. The results of PC and PFA are within the same range as reported by McCarter et al. (2012) and Nanukuttan et al. (2017a). It highlights that the presence of microsilica in MS concrete altered the pore structure (McCarter et al. 2012). Further, not much variation is observed in

the two samples for each mixture, nor at each depth of the three concrete mixtures, as was reported by McCarter et al. (2012). Therefore, the calculated values for E_a/R_g for each mixture can be used to correct the resistance data to a reference temperature of 25°C using Eq. (2). The standardized resistance (SR) values for each concrete mixture were then averaged for the two concrete blocks and presented in Fig. 5.

It can be seen from the SRs in Fig. 5(a) to (c) that the huge fluctuations of the as-measured resistance in Fig. 2 are now slightly reduced, which indicates the removal of temperature effects from the measurement, as established by McCarter et al. (2012). However, from Fig. 5(c), it can be observed that there are still diurnal variations occurring after 80 days. Electrical resistance is also affected by other environmental interactions, such as ambient temperature, rainfall, and

Table 3—E_a/R_g determined from Eq. (3) and activation energy, E_a

	Mixtures											
	PC1		PC2		PFA1		PFA2		MS1		MS2	
Depth	E_a/R_g, K	E_a, kJ/M	E_a/R_g, K	E_a, kJ/M	E_a/R_g, K	E_a, kJ/M	E_a/R_g, K	E_a, kJ/M	E_a/R_g, K	E_a, kJ/M	E_a/R_g, K	E_a, kJ/M
15 mm	3.92	32.61	4.87	40.48	5.70	47.42	4.51	37.53	6.42	53.41	6.02	50.04
25 mm	4.50	37.38	5.43	45.15	5.44	45.24	5.24	43.57	6.87	57.10	6.67	55.48
45 mm	5.40	44.86	5.40	44.90	5.69	47.31	5.33	44.33	6.29	52.26	6.42	53.38
Average	4.60	38.28	5.23	43.51	5.61	46.66	5.03	41.81	6.53	54.26	6.37	52.97
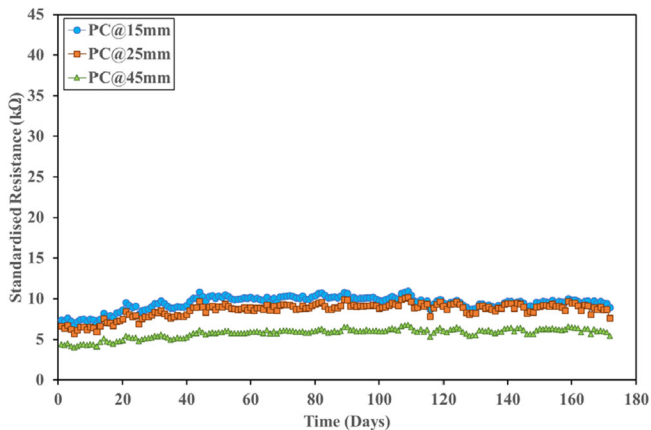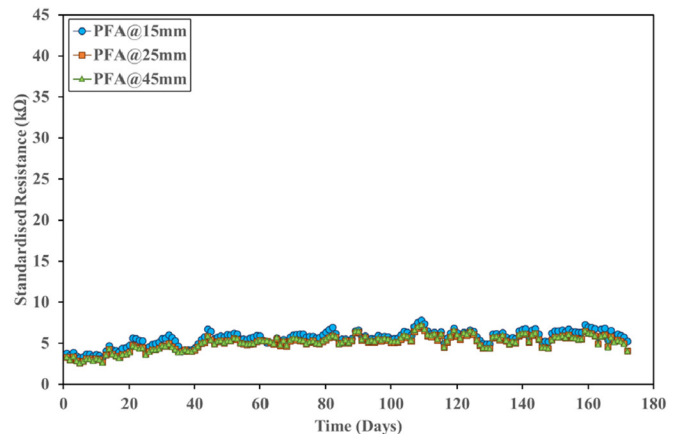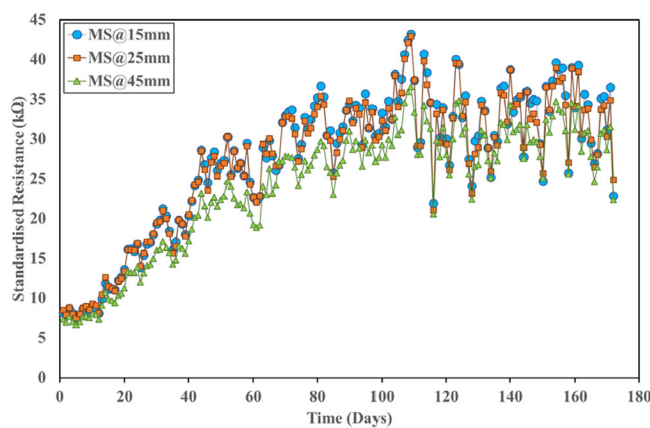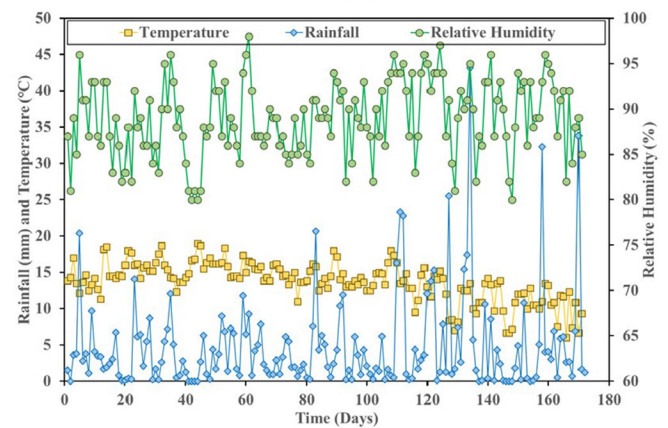
Fig. 5—Standardized resistance (kΩ) to reference temperature of 25°C for: (a) PC concrete mixture; (b) PFA concrete mixture; (c) MS concrete mixture; (d) rainfall, RH, and ambient temperature data during studied period as per UK met office.

relative humidity (RH) (Azarsa and Gupta 2017). Figure 5(d) shows the rainfall and ambient temperature data from the UK Met Office (metoffice.gov.uk). When comparing these data with the MS data in Fig. 5(c), it is clear that the resistance decrease can be attributed to the increase in rainfall and the associated possible increase in the moisture uptake. However, with no RH sensors installed in the concrete specimen, the effect of moisture variation on electrical resistance could not be fully quantified.

Determination of diffusion coefficient D_e

As discussed in the previous section, the performance of concrete can be assessed based on electrical resistance, chloride diffusion, and permeability. However, the electrical resistance of the saturated concrete can be used to determine the diffusivity (Hossain and Lachemi 2004; McCarter et al. 2012; Basnayake et al. 2020). Garboczi and Bentz (1992) presented an inverse relationship between the diffusion coefficient of a porous material and the bulk resistivity of the saturated material

$$\frac{D_e}{D_0} = \frac{\rho}{\rho_{bulk}} \tag{4}$$

where D_0 is the diffusion coefficient of the desired ion in pure water (for chloride, $D_0 = 2.032 \times 10^{-9}$ m²/s); ρ is the resistivity of pore fluid (estimated using the NIST model); and ρ_{bulk} is the bulk resistivity of the saturated material. ρ_{bulk} can be obtained from the steady-state condition of the SR for the three concretes. Therefore, it is necessary to determine the steady-state electrical resistance values for the three concretes from a large number of data sets.

Automated piecewise linear regression for SHM data

It can be observed from Fig. 5 that the resistance increases with time for the three concrete types. It can also be observed that there is a change in the slope of resistance with time. For example, in the case of PC at 15 mm depth from the exposed surface, the resistance increases from 8 to 10 kΩ in the first 15 days, and then there is a drop in resistance. Again, the resistance starts to increase at a faster rate, rising from 8 to 12 kΩ during the initial 110 days, and subsequently, it nearly stabilizes. In the case of PFA at 15 mm depth, there is a drop in resistance after day 12, and then it starts to increase at a faster rate, rising from 5 to 8 kΩ in 110 days, and it nearly stabilizes in the remaining days. Similarly, it can be observed for MS at 15 mm depth that the resistance drops at approximately 14 days and then starts increasing significantly. The resistance increases from 10 to 35 kΩ in 80 days, and later, it increases at a slower rate. A similar trend can be seen for all the depths plotted in Fig. 5 for PC, PFA, and MS. During the cement hydration process, there are significant changes in the concrete microstructure as the liquid state of cement is changed to a hardened state. As a result, there are changes in mechanical properties and behavioral patterns in the early age of concrete (Glišić and Simon 2000). In addition, the increase in resistance with time is also a result of the microstructural changes due to the hydration of PC and the pozzolanic reactions of PFA and MS. The resistance

increases initially with these reactions and either increases at a slower rate or stabilizes when these reactions either slow down or stop (McCarter et al. 2012). After this stage, the resistance decreases only when the concrete starts to deteriorate (Neville 2011; Cosoli et al. 2020). Therefore, in the current study, the SR graphs for each mixture are studied to determine the rate of change in resistance, the time taken to stabilize the resistance, and the stabilized resistance value. It is also necessary to understand and identify the changes in the early age of concrete from the data and its influence on the long-term service life performance.

It is interesting to note that the resistance data is subdivided into smaller disjointed regions, showing the change in the behavior of the resistance data. One of the solutions for addressing this situation was to divide the data into k-many clusters and fit a continuous linear regression to different clusters and, thus, perform a PLR (Ferrari-Trecate and Muselli 2002). PLR is used to partition the independent variables into smaller regions and fit a separate segment for each region to define the change in the behavior of the variables (Muhammad et al. 2014). The breakpoint of these regions could determine the change in the gradient of the resistance and the time taken to stabilize the resistance. Therefore, to proceed with the analysis, an ACPLR approach was used to understand and interpret the SR data and reach the solution to the problem, as described in the following.

Step 1: Gaussian weighted moving average (GWMA) filter—One of the main problems with analyzing SHM data using PLR was the noise in the data. As the concrete specimens were exposed to the outdoor environment, they were subjected to rain, humidity, temperature, and other environmental effects. Although the influence of temperature was reduced from the resistance measurements, the data still seem noisy and, hence, can affect the predictions. A GWMA filter was used to compress the noise level of the original data, thereby smoothing the noisy data and reflecting the trend of the original data. This was done by selecting a window of a few data points to extract the noise and then assuming that for the distribution, the mean is zero with standard deviation σ to scale the noise level (Yavuz and Safak 2019). However, there is no straightforward rule for selecting a smoothing window. A short window size is usually selected to extract high-frequency data, while a long smoothing window is selected to extract low-frequency data and may eliminate high-frequency data points (Takatoi et al. 2020). This is explained by considering one data set for MS concrete at 15 mm depth, as shown in Fig. 6(a). As only a few noisy points can be seen in the data, a short window size was chosen to smooth noisy data and maintain an optimum signal-to-noise ratio, as shown in Fig. 6(a).

Step 2: k-means clustering—It is an unsupervised ML algorithm that identifies patterns within the data sets without any training data or manual input and provides exploratory analysis (Hearty 2016). The main objective of using a k-means clustering algorithm is to separate the data set into clusters, find optimal coefficients, and predict the best possible outcome corresponding to a large number of data points that were difficult to predict manually. The algorithm was selected due to its advantage of dealing with large data
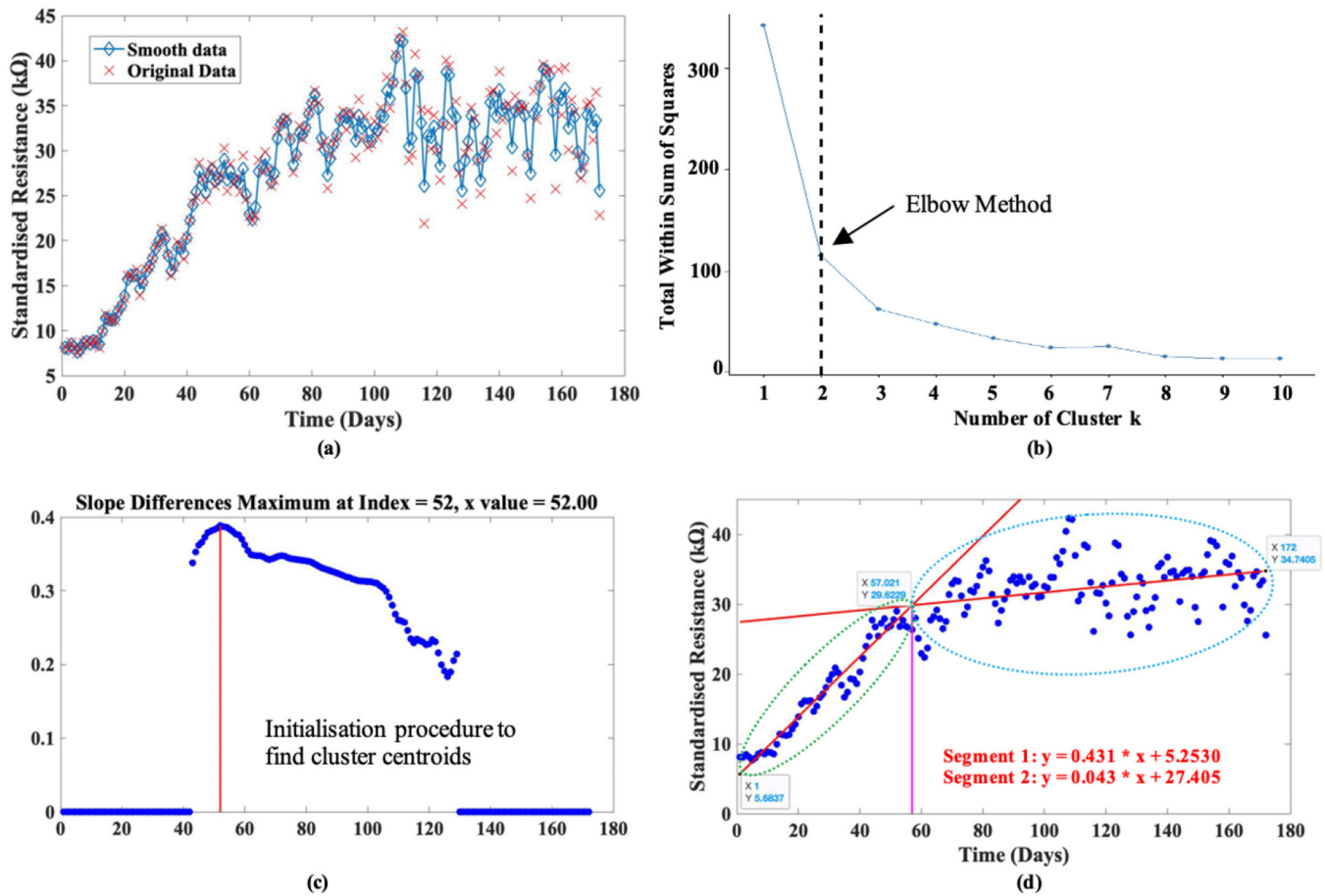
Fig. 6—Steps for ACPLR: (a) original data versus smoothed data (GWMA filter) for MS at 15 mm depth; (b) identifying number of optimal clusters using elbow method; (c) identification of maximum slope difference to find final clusters; and (d) piecewise linear regression on two clusters and breakpoint showing change in resistance, stabilized resistance, and time taken to stabilize resistance. (Note: Process was carried out 18 times [nine times each for short-term and long-term data analysis] in the study.)

sets and running multiple clustering configurations to extract key content (Hearty 2016).

First, the elbow curve method was also used to identify the optimal number of clusters k. The algorithm was run for different values of k ranging from 1 to 10, and then the sum of squared distances to the centroid across all data points for each value of k was calculated. After plotting these points, the point where the average distance from the centroid falls suddenly was identified to find the optimal k clusters, as shown in Fig. 6(b). Thus, two clusters were specified for the analysis.

The next step was to provide an approximate location of the breakpoint such that there are at least 25% of the points in one cluster to have a good estimate of the line. The algorithm divided the data into approximate clusters from the approximate location of the breakpoint to get the accurate location of the breakpoint. After initializing the algorithm, new cluster centroids were redefined by extracting the slope difference from the structure array. Based on this, the maximum slope difference was identified, as shown in Fig. 6(c), and thus, the two accurate clusters were found such that the data points were then kept to either side of the maximum slope difference.

Step 3: Piecewise linear regression—After obtaining the accurate location of the clusters, the algorithm estimated the

position of the breakpoint and performed piecewise linear regression for each cluster simultaneously to have minimal absolute deviation (Yang et al. 2016). The linear coefficients and the intercept of linear functions were obtained by solving linear regression for each cluster, as shown in Fig. 6(d). Finally, the interaction point for the segments was identified and considered as the ultimate breakpoint for the change in resistance. The intersection point (x, y) was considered as the time taken to stabilize the resistance value (x-axis = 57 days) and the stabilized resistance (y-axis = 29.63 kΩ). Figure 6(d) shows the change in the resistance through two new clusters and linear regression for the two clusters via ACPLR for MS at a depth of 15 mm from the surface.

This paper uses the developed ACPLR-based SHM methodology in two phases for an effective and reliable interpretation of the resistance data. In the first phase, short-term (early-age) resistance data up to 21 days were used to see the early change in resistance due to curing and identify the time taken to develop a discontinuous capillary pore structure during wet curing. The second phase used the complete resistance data to determine the standard steady-state conditions for resistance and diffusion coefficient to predict concrete performance.

RESULTS AND DISCUSSION
Phase 1—Short-term data analysis using ACPLR

As discussed in the last section, there was a change in the resistance during the initial few days of curing, and then the resistance started to increase at a faster rate for all depths in all three types of concrete. The change in resistance at an early age depicts the time taken for the concrete to develop its pore structure and start influencing the physical and mineralogical characteristics; both would contribute to the development of a discontinuous pore structure. According to Basnayake et al. (2020), the time taken to develop this discontinuous capillary pore structure can be identified from the change in slope of the resistance with time. That is, the intersection point of the two segments is considered to demonstrate the minimum time at which the wet curing influences the microstructure of the three concretes. The ACPLR is performed for the initial 21 days to study the change in behavior of concrete due to early-age hydration and curing effect. Table 4 shows both the intersection point at which the resistance starts to increase again and the change in the gradient of resistance.

It can be seen that the intersection point is at 5.18 days for PC, 5.85 days for PFA, and 6.31 days for MS. As the water content for the three concretes is the same (145 kg/m^3), at least 5.5, 6, and 7 days, respectively, are required for PC, PFA, and MS concretes to begin to develop a discontinuous pore structure to satisfy durability requirements. These results are in agreement with Basnayake et al. (2020) that there is a change in resistance before and after obtaining a discontinuous pore structure, and wet curing should be continued for at least 7 days until the pore structure develops discontinuous pores. However, it is important to recognize that this suggested minimum wet curing duration is not universally applicable and may vary for different cementitious materials. In addition, Table 4 shows that MS takes the largest time to obtain a discontinuous pore structure, followed by PFA and PC. However, there is not much difference in the minimum wet curing duration for the three concretes, suggesting that all concretes started developing discontinuous pores almost simultaneously. This is likely because, during the very early stage of portland cement hydration, there is little effect of the pozzolanic reaction (Zelić et al. 2000).

Phase 2—Long-term data analysis using ACPLR

The second phase of the analysis was done to determine the steady-state conditions for the three concrete types and, thereby, to estimate diffusion coefficients to predict the concretes' performance. The ACPLR was performed for the complete data set. Table 5 shows the initial rate of increase in resistance, the value of stabilized resistance, and the time taken to stabilize resistance based on the outputs from the program. The diffusion coefficient values were then calculated using the stabilized resistance values as ρ_{bulk} in the relationship described by Garboczi and Bentz (1992) in Eq. (4).

Overall trends—It is observed that, overall, the resistance increased with time for all concrete types, showing that the pore structure is getting less conductive with time. Figure 7(a) presents the change in resistance with time for the three concretes at 15, 25, and 45 mm depths from the

Table 4—Change in resistance at early age and intersection point for two segments

Concrete mixture	Depth of sensor, mm	Change in resistance, %	Intersection point, days	Resistance, kΩ
PC	15	16.6	5.18	8.21
	25	13.4	4.95	5.71
	45	10.9	4.62	4.03
PFA	15	26.4	5.85	3.33
	25	18.8	4.84	2.81
	45	16.8	4.76	2.79
MS	15	65.9	6.31	7.05
	25	57.7	5.63	7.68
	45	52.5	5.54	6.47

(a)

(b)
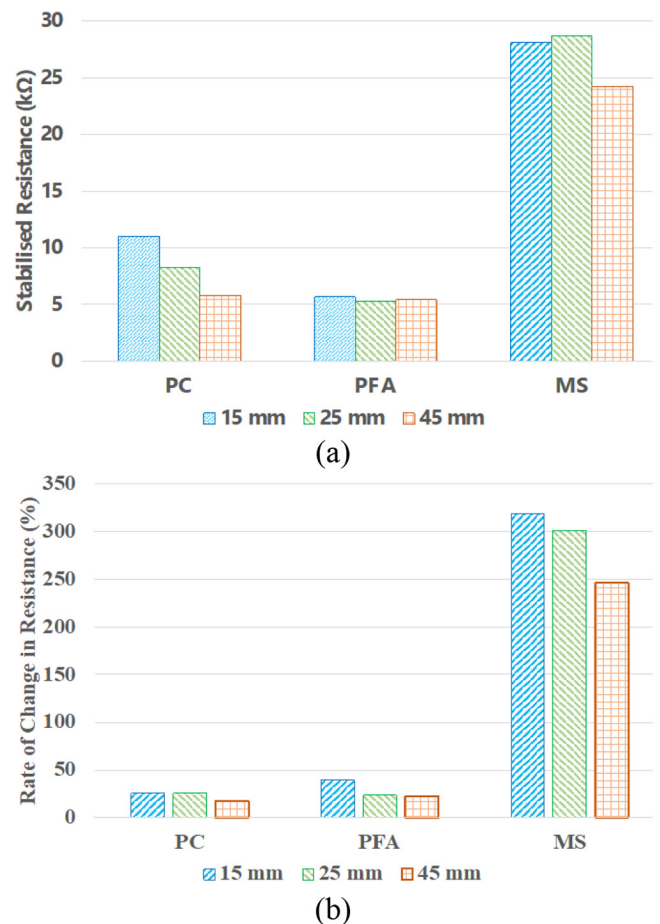
Fig. 7—(a) Rate of change in resistance; and (b) stabilized resistance for three concretes at three different depths determined using ACPLR.

concrete surface. The rate of increase in resistance is the highest for MS, followed by PFA and PC. The data in Table 5 shows that at 15 mm depth, MS has the highest initial resistance, which is approximately five times that of the PFA. The initial resistance values varied for the three concretes and are within the range of one to five times that of the PC. Similarly, MS took more time to stabilize when compared to both PFA and PC, as shown in Fig. 7(b). The addition of SCMs such as microsilica and PFA alters the pore structure

Table 5—Determination of steady-state resistance/diffusion coefficient values using ACPLR

Concrete mixture	Depth, mm	Rate of increase in resistance, %	Time taken to stabilize resistance, days	Stabilized resistance value, kΩ	Diffusion coefficient, $\times 10^{-12}$ m^2/s	Average diffusion coefficient, $\times 10^{-12}$ m^2/s
PC	15	25.6	49.62	11.02	1.11	
	25	25.8	49.77	8.32	1.46	1.56
	45	17.4	50.77	5.78	2.11	
PFA	15	39.1	43.76	5.68	2.45	
	25	23.5	49.76	5.28	2.64	2.55
	45	22.6	52.32	5.42	2.57	
MS	15	318.5	56.09	28.10	1.08	
	25	3301.2	56.91	28.72	1.05	1.12
	45	246.2	58.52	24.27	1.24	

due to the continued pozzolanic reactivity of the binder material in all concrete and increases the rate of change in resistance for MS (Safiuddin et al. 2007; Nanukuttan et al. 2015). Further, microsilica is a denser material and quickly reacts with the portland cement hydration products in a pozzolanic reaction than PFA once the discontinuous capillary pore structure starts to develop. Therefore, it leads to a significant reduction in the porosity of concrete, resulting in a substantial increase in resistance (Sellevold and Radjy 1983; Berke 1988).

Depth effect—Figure 7(b) shows that the resistance at the deeper concrete (45 mm) is lower than at the exposed surface (15 mm) for the three concretes. Similarly, all concretes took more time to stabilize at the deeper part. This is primarily due to the drying and wetting effects of the concretes. Resistance is strongly affected by the interaction occurring between the surface layer of concrete and the atmosphere (McCarter et al. 2005). While the deeper part of the concrete is saturated, the surface releases more moisture, so the evaporation of moisture increases the surface layer's resistance. However, in the case of MS, the resistance nearer to the surface at a depth of 15 mm is lower than at a depth of 25 mm. This may be due to the decrease in resistance caused by water being trapped during the pozzolanic reaction of the binder material in the MS concrete.

Diffusion coefficient—Table 5 shows the estimated diffusion coefficient values for the three mixtures using the stabilized resistance values. It is observed that the diffusion coefficients have a trend opposite to that of the resistance values, as is expected. The continued hydration and pozzolanic reactions reduce both the porosity and the connected porosity in concrete; thus, the overall diffusion coefficient reduces with time (Oslakovic et al. 2008). The calculated values of the diffusion coefficient can then be used to predict the performance of concrete and thereby the service life. Table 5 shows that the best performance among the three concretes is observed for MS. However, confirming this requires further research to determine their durability performance, which is outside the scope of this paper.

Advantages of using ACPLR-based SHM methodology

a) The ACPLR-SHM methodology used for the analysis is an easy and understandable approach to interpret large amounts of complex data by identifying the best aspects of segmented regression. Each line segment identified from the algorithm is balanced against the noise such that it reduces the influence of short-term fluctuations to show long-term results in smooth data. The algorithm efficiently analyzed a large amount of noisy electrical resistance sensor data (24,000 data points) to obtain a steady-state condition of resistance.

b) This approach is more efficient than the conventional method for different types of concrete and exposure conditions to calculate the value of the diffusion coefficient. The value of the diffusion coefficient is either determined by performing nondestructive testing of concretes in the lab or using an assumed diffusion coefficient value from the literature for service life modeling. Thus, this proposed methodology provides valuable knowledge on stabilized resistance values that can be used to calculate diffusion coefficient values.

c) The proposed methodology provides reliable interpretations of the resistance/diffusion coefficient values. The obtained values of diffusion coefficient for the three concretes are in the range of 1 to 3×10^{-12} m^2/s, which is at the high end of the spectrum for good-quality and high-performance concrete as per the literature to measure the performance of the concrete (Bjegović et al. 1995; Yang et al. 2018). Therefore, this criterion can be used as a measure of the performance of the concrete and thereby reinforce the reliability of the proposed methodology.

CONCLUSIONS

The novelty of the proposed methodology lies in its ability to smooth noisy data and perform automated clustering-based piecewise linear regression (ACPLR) on the data set to obtain the time taken to develop a discontinuous pore structure, time taken to stabilize resistance, the stabilized resistance value, and the rate of change in resistance. Based on the results obtained from the application of ACPLR to electrical resistance sensor data, it can be concluded that the proposed methodology diminished the challenges of handling, smoothing, and analyzing large data sets manually.

The methodology is robust enough to provide some valuable insights on the steady-state condition of the resistance, which means interpretability is of importance and thereby can be further used for calculating the diffusion coefficient values. The stabilized resistance and diffusion coefficient values obtained from the structural health monitoring (SHM) data also demonstrated the benefit of using supplementary cementitious materials (SCMs) to improve the durability of concrete. Overall, practitioners and researchers can use the proposed ACPLR-based SHM methodology to interpret resistance sensor data for different types of concrete structures for monitoring and determining the resistance/diffusion coefficient values and thereby predict the performance of concrete in structures.

FURTHER RESEARCH

The results from the study highlighted that even after reducing the influence of temperature on resistance measurements, other environmental conditions, such as ambient temperature, RH, and rainfall also had an impact on the resistance measurements. Therefore, it is suggested that future work should use RH sensors inside and outside the concrete and temperature sensors outside the concrete during SHM and consider their effect on reducing the influence of ambient environmental conditions.

The proposed ACPLR-based SHM methodology was applied to the resistance sensor data from the concrete blocks exposed to environmental conditions for only 6 months. To conduct a more thorough evaluation of the methodology, it is suggested that a long-term study should be conducted across a wider set of locations with marine conditions.

AUTHOR BIOS
ACI member **Harshita Garg** *is a Doctorate Student at the School of Civil Engineering, University of Leeds, Leeds, UK. She received her bachelor's degree in architecture from India and her MSc. (Eng.) in international construction management and engineering from the University of Leeds. Her research interests include structural health monitoring, performance of concrete structures, service life prediction, and maintenance management of civil infrastructure.*

Kai Yang *is an Associate Professor in the College of Materials Science and Engineering, Chongqing University, Chongqing, China. He received his bachelor's and master's degrees from Chongqing University, and his PhD from Queen's University Belfast, Belfast, UK. His research interests include durability assessment of structures, structural health monitoring, alkali-activated cementitious materials, and the development of nondestructive tests for assessing concrete.*

Anthony G. Cohn *is a Professor at the School of Computing, University of Leeds. He received his BSc and PhD from the University of Essex, Essex, UK. His research interests include artificial intelligence, knowledge representation and reasoning, data and sensor fusion, cognitive vision, spatial representation and reasoning, and robotics.*

Duncan Borman *is an Associate Professor at the University of Leeds, where he received his MSc and PhD. His research interests include computational fluid dynamics and mathematical modeling of environmental and multiphase flows, particularly those with industrial applications.*

Sreejith V. Nanukuttan *is a Senior Lecturer at the School of Natural and Built Environment, Queens University Belfast, where he received his PhD. His research interests include testing and monitoring of structures, durability of structures, and service-life prediction.*

P. A. Muhammed Basheer, *FACI, is a Professor of civil engineering and the Executive Dean of the School of Energy, Geoscience, Infrastructure and Society at Heriot-Watt University, Edinburgh, UK. He received his PhD and DSc from Queen's University Belfast. He is a member of ACI Committees 130, Sustainability of Concrete; 201, Durability of Concrete; 211, Proportioning Concrete Mixtures; 236, Material Science of Concrete; 365, Service Life Prediction; and 444, Structural Health Monitoring. His research interests include the durability of concrete, nondestructive tests, structural health monitoring, performance of materials in structures, and service life prediction.*

NOTATION

D_0 = diffusion coefficient of chloride ion in pure water
E_a = activation energy, kJ/mol
R_g = universal gas constant, 8.3141×10^{-3} kJ/mole/K
ρ = resistivity of pore fluid
ρ_0 = pre-exponential constant, kΩ
ρ_{bulk} = bulk resistivity of saturated material
ρ_x = equivalent resistance, kΩ, at reference temperature 25°C
ρ_y = resistance, kΩ, recorded at the temperature at $T_{k,x}$

REFERENCES
ACI Committee 201, 2016, "Guide to Durable Concrete (201.2R-16)," American Concrete Institute, Farmington Hills, MI, 84 pp.

ACI Committee 444, 2021, "Structural Health Monitoring Technologies for Concrete Structures—Report (ACI PRC-444.2-21)," American Concrete Institute, Farmington Hills, MI, 110 pp.

Ahmed, Z.; Ali, J. S. M.; Rafeeq, M.; and Hrairi, M., 2019, "Application of Machine Learning with Impedance Based Techniques for Structural Health Monitoring of Civil Infrastructure," *International Journal of Innovative Technology and Exploring Engineering (IJITEE)*, V. 8, No. 6S4, pp. 1139-1148.

Aydin, K., and Kisi, O., 2015, "Damage Diagnosis in Beam-Like Structures by Artificial Neural Networks," *Journal of Civil Engineering and Management*, V. 21, No. 5, pp. 591-604. doi: 10.3846/13923730.2014.890663

Azarsa, P., and Gupta, R., 2017, "Electrical Resistivity of Concrete for Durability Evaluation: A Review," *Advances in Materials Science and Engineering*, pp. 1-30. doi: 10.1155/2017/8453095

Ballo, F.; Gobbi, M.; Mastinu, G.; and Previati, G., 2014, "Advances in Force and Moments Measurements by an Innovative Six-Axis Load Cell," *Experimental Mechanics*, V. 54, No. 4, pp. 571-592. doi: 10.1007/s11340-013-9824-4

Basheer, P. A. M.; Gilleece, P. R. V.; Long, A. E.; and Mc Carter, W. J., 2002, "Monitoring Electrical Resistance of Concretes Containing Alternative Cementitious Materials to Assess Their Resistance to Chloride Penetration," *Cement and Concrete Composites*, V. 24, No. 5, pp. 437-449. doi: 10.1016/S0958-9465(01)00075-0

Basheer, P. A. M.; Grattan, K. T.; Sun, T.; Long, A. E.; McPolin, D.; and Xie, W., 2004, "Fiber Optic Chemical Sensor Systems for Monitoring pH changes in Concrete," *Advanced Environmental, Chemical, and Biological Sensing Technologies II*, International Society for Optics and Photonics, Bellingham, WA, pp.144-153.

Basnayake, K.; Mazumder, A. F.; Attanayake, U.; and Berke, N. S., 2020, "Assessment of Concrete Curing Duration using Bulk Electrical Conductivity and Porosity," *Transportation Research Record: Journal of the Transportation Research Board*, V. 2674, No. 10, pp. 261-268. doi: 10.1177/0361198120935114

Berke, N. S., 1988, "Microsilica and Concrete Durability," *Transportation Research Record: Journal of the Transportation Research Board*, V. 1204, pp. 21-26.

Bjegović, D.; Krstić, V.; Mikulić, D.; and Ukrainczyk, V., 1995, "C-D-c-t Diagrams for Practical Design of Concrete Durability Parameters," *Cement and Concrete Research*, V. 25, No. 1, pp. 187-196. doi: 10.1016/0008-8846(94)00126-J

Brownjohn, J. M. W.; de Stefano, A.; Xu, Y. L.; Wenzel, H.; and Aktan, A. E., 2011, "Vibration-Based Monitoring of Civil Infrastructure: Challenges and Successes," *Journal of Civil Structural Health Monitoring*, V. 1, No. 3-4, pp. 79-95.

Bungey, J. H.; Millard, S. G.; and Grantham, M. G., 2006, *Testing of Concrete in Structures*, fourth edition, Taylor & Francis, New York, 352 pp.

Chandrasekaran, S., 2019, "Structural Health Monitoring: An Overview," *Structural Health Monitoring with Application to Offshore Structures*, World Scientific, pp. 1-50.

Cosoli, G.; Mobili, A.; Tittarelli, F.; Revel, G. M.; and Chiariotti, P., 2020, "Electrical Resistivity and Electrical Impedance Measurement in Mortar and Concrete Elements: A Systematic Review," *Applied Sciences*, Basel, Switzerland, V. 10, No. 24, pp. 1-42. doi: 10.3390/app10249152

Demircilioğlu, E.; Teomete, E.; Schlangen, E.; and Baeza, F. J., 2019, "Temperature and Moisture Effects on Electrical Resistance and Strain Sensitivity of Smart Concrete," *Construction and Building Materials*, V. 224, No. 11, pp. 420-427. doi: 10.1016/j.conbuildmat.2019.07.091

Diez, A.; Khoa, N. L. D.; Makki Alamdari, M.; Wang, Y.; Chen, F.; and Runcie, P., 2016, "A Clustering Approach for Structural Health Monitoring on Bridges," *Journal of Civil Structural Health Monitoring*, V. 6, No. 3, pp. 429-445. doi: 10.1007/s13349-016-0160-0

Dong, C. Z., and Catbas, F. N., 2021, "A Review of Computer Vision-Based Structural Health Monitoring at Local and Global Levels," *Structural Health Monitoring*, V. 20, No. 2, pp. 692-743. doi: 10.1177/1475921720935585

Fabo, P.; Sedivy, S.; Kuba, M.; Buchholcerova, A.; Dudak, J.; and Gaspar, G., 2020, "PLC Based Weather Station for Experimental Measurements," *19th International Conference on Mechatronics – Mechatronika (ME)*, Prague, Czech Republic, pp. 1-4.

Farrar, C. R., and Worden, K., 2012, *Structural Health Monitoring: A Machine Learning Perspective*, first edition, John Wiley & Sons, Ltd, Chichester, UK, 631 pp.

Ferrari-Trecate, G., and Muselli, M., 2002, "A New Learning Method for Piecewise Linear Regression," J. R. Dorronsoro, ed., *Artificial Neural Networks – ICANN 2002, International Conference*, Springer Verlag, Madrid, Spain, pp. 444-449.

Flah, M.; Nunez, I.; Ben Chaabene, W.; and Nehdi, M. L., 2021, "Machine Learning Algorithms in Civil Structural Health Monitoring: A Systematic Review," *Archives of Computational Methods in Engineering*, V. 28, No. 4, pp. 2621-2643. doi: 10.1007/s11831-020-09471-9

Frangopol, D. M., and Kim, S., 2014, "Prognosis and Life-Cycle Assessment Based on SHM Information," *Sensor Technologies for Civil Infrastructures. Volume 2 - Applications in Structural Health Monitoring*, M. L. Wang, J. P. Lynch, and H. Sohn, eds., Woodhead Publishing, Netherlands, pp. 145-171.

Garboczi, E. J., and Bentz, D. P., 1992, "Computer Simulation of the Diffusivity of Cement-Based Materials," *Journal of Materials Science*, V. 27, No. 8, pp. 2083-2092. doi: 10.1007/BF01117921

Glišić, B., and Simon, N., 2000, "Monitoring of Concrete at Very Early Age Using Stiff SOFO Sensor," *Cement and Concrete Composites*, V. 22, No. 2, pp. 115-119. doi: 10.1016/S0958-9465(99)00037-2

Hearty, J., 2016, *Advanced Machine Learning with Python*, first edition, Packt Publishing, Birmingham, UK, 278 pp.

Hernandez, W., 2006, "Improving the Response of a Load Cell by Using Optimal Filtering," *Sensors (Basel)*, V. 6, No. 7, pp. 697-711. doi: 10.3390/s6070697

Hossain, K. M. A., and Lachemi, M., 2004, "Corrosion Resistance and Chloride Diffusivity of Volcanic Ash Blended Cement Mortar," *Cement and Concrete Research*, V. 34, No. 4, pp. 695-702. doi: 10.1016/j.cemconres.2003.10.021

Jansen, D.; Goetz-Neunhoeffer, F.; Lothenbach, B.; and Neubauer, J., 2012, "The Early Hydration of Ordinary Portland Cement (OPC): An Approach Comparing Measured Heat Flow with Calculated Heat Flow from QXRD," *Cement and Concrete Research*, V. 42, No. 1, pp. 134-138. doi: 10.1016/j.cemconres.2011.09.001

Kalkani, E. C., 1992, "Ambient Temperature Effect in Concrete Dam Foundation Seepage," *Journal of Geotechnical Engineering*, ASCE, V. 118, No. 1, pp. 1-11. doi: 10.1061/(ASCE)0733-9410(1992)118:1(1)

Karbassi, A.; Mohebi, B.; Rezaee, S.; and Lestuzzi, P., 2014, "Damage Prediction for Regular Reinforced Concrete Buildings using the Decision Tree Algorithm," *Computers and Structures*, V. 130, pp. 46-56. doi: 10.1016/j.compstruc.2013.10.006

McCarter, W. J.; Chrisp, T. M.; Starrs, G.; Adamson, A.; Owens, E.; Basheer, P. A. M.; Nanukuttan, S. V.; Srinivasan, S.; and Holmes, N., 2012, "Developments in Performance Monitoring of Concrete Exposed to Extreme Environments," *Journal of Infrastructure Systems*, ASCE, V. 18, No. 3, pp. 167-175. doi: 10.1061/(ASCE)IS.1943-555X.0000089

McCarter, W. J.; Chrisp, T. M.; Starrs, G., Basheer, P. A. M.; and Blewett, J., 2005, "Field Monitoring of Electrical Conductivity of Cover-Zone Concrete," *Cement and Concrete Composites*, V. 27, No. 7-8, pp. 809-817.

Montemor, M. F.; Alves, J. H.; Simões, A. M.; Fernandes, J. C. S.; Lourenço, Z.; Costa, A. J. S.; Appleton, A. J.; and Ferreira, M. G. S., 2006, "Multiprobe Chloride Sensor for In-Situ Monitoring of Reinforced Concrete Structures," *Cement and Concrete Composites*, V. 28, No. 3, pp. 233-236. doi: 10.1016/j.cemconcomp.2006.01.005

Muhammad, Y., S.; Afgan, N.; Iqbal, M.; and Hussain, I., 2014, "Modeling Non-linear Behavior of Independent Variables," *International Journal of Business and Social Science*, V. 5, No. 13, pp. 192-200.

Nanukuttan, S. V.; Basheer, P. A. M.; McCarter, W. J.; Tang, L.; Holmes, N.; Chrisp, T. M.; Starrs, G.; and Magee, B., 2015, "The Performance of Concrete Exposed to Marine Environments: Predictive Modelling and Use of Laboratory/On-Site Test Methods," *Construction and Building Materials*, V. 93, pp. 831-840. doi: 10.1016/j.conbuildmat.2015.05.083

Nanukuttan, S. V.; Campbell, L.; Mccarter, J.; Basheer, M.; Mcrobert, J.; and McBurney, P., 2017a, "State of Health Assessment of Concrete Repair using Electrical Sensors," *2nd International RILEM/COST Conference on Early Age Cracking and Serviceability in Cement-Based Materials and Structures*, S. Staquet, and D. Aggelis, eds., RILEM Publications SARL, Brussels, pp. 149-154.

Nanukuttan, S. V.; Yang, K.; McCarter, J.; and Basheer, P. A. M., 2017b, "Methods of Assessing the Durability and Service Life of Concrete Structures," *Annual Technical Symposium of the Institute of Concrete Technology (ICT)*, Leeds, UK, pp. 1-14.

Nehdi, M. L., and Soliman, A. M., 2011, "Early-Age Properties of Concrete: Overview of Fundamental Concepts and State-of-the-Art Research," *Construction Materials*, V. 164, No. 2, pp. 57-77.

Neville, A. M., 2011, *Properties of Concrete*, fifth edition, Pearson Education Limited, London, UK, 846 pp.

Nokken, M. R., and Hooton, R. D., 2007, "Using Pore Parameters to Estimate Permeability or Conductivity of Concrete," *Materials and Structures*, V. 41, No. 1, pp. 1-16. doi: 10.1617/s11527-006-9212-y

Oslakovic, I. S.; Serdar, M.; Bjegovic, D.; and Mikulic, D., 2008, "Modeling of Time Depended Changes of Chloride Diffusion Coefficient," *11DBMC International Conference on Durability of Building Materials and Components*, Istanbul, Turkey, pp. 203-2112.

Pan, Y., and Zhang, L., 2021, "Roles of Artificial Intelligence in Construction Engineering and Management: A Critical Review and Future Trends," *Automation in Construction*, V. 122, No. 2, pp. 1-21. doi: 10.1016/j.autcon.2020.103517

Perveen, K.; Bridges, G. E.; Bhadra, S.; and Thomson, D. J., 2014, "Corrosion Potential Sensor for Remote Monitoring of Civil Structure based on Printed Circuit Board Sensor," *IEEE Transactions on Instrumentation and Measurement*, V. 63, No. 10, pp. 2422-2431. doi: 10.1109/TIM.2014.2310092

Rai, V. K., 2007, "Temperature Sensors and Optical Sensors," *Applied Physics B: Lasers and Optics*, V. 88, No. 2, pp. 297-303. doi: 10.1007/s00340-007-2717-4

Safiuddin, M.; Raman, S. N.; and Zain, M. F. M., 2007, "Effect of Different Curing Methods on the Properties of Microsilica Concrete," *Australian Journal of Basic and Applied Sciences*, V. 1, No. 2, pp. 87-95.

Schöler, A.; Lothenbach, B.; Winnefeld, F.; Haha, M. B.; Zajac, M.; and Ludwig, H.-M., 2017, "Early Hydration of SCM-Blended Portland Cements: A Pore Solution and Isothermal Calorimetry Study," *Cement and Concrete Research*, V. 93, pp. 71-82. doi: 10.1016/j.cemconres.2016.11.013

Scrivener, K. L., and Nonat, A., 2011, "Hydration of Cementitious Materials, Present and Future," *Cement and Concrete Research*, V. 41, No. 7, pp. 651-665. doi: 10.1016/j.cemconres.2011.03.026

Sellevold, E. J., and Radjy, F. F., 1983, Condensed Silica fume (Microsilica) in Concrete: Water Demand and Strength Development, *Symposium Paper*, V. 79, pp. 677-694.

Smarsly, K.; Dragos, K.; and Wiggenbrock, J., 2016, "Machine Learning Techniques for Structural Health Monitoring," *8th European Workshop on Structural Health Monitoring (EWSHM)*, Bilbao, Spain, pp. 1522-1531.

Steinhart, J. S., and Hart, S. R., 1968, "Calibration Curves for Thermistors," *Deep-Sea Research and Oceanographic Abstracts*, V. 15, No. 4, pp. 497-503. doi: 10.1016/0011-7471(68)90057-0

Takatoi, G.; Sugawara, T.; Sakiyama, K.; and Li, Y., 2020, "Simple Electromagnetic Analysis against Activation Functions of Deep Neural Networks," J. Zhou, ed., *International Conference on Applied Cryptography and Network Security*, Springer, Cham, pp.181-197.

Tanner, B. D., 1990, "Automated Weather Stations," *Remote Sensing Reviews*, V. 5, No. 1, pp. 73-98. doi: 10.1080/02757259009532123

Yang, K.; Basheer, P. A. M.; Bai, Y.; Magee, B. J.; and Long, A. E., 2014, "Development of a New In-Situ Test Method to Measure the Air Permeability of High-Performance Concretes," *NDT & E International*, V. 64, pp. 30-40. doi: 10.1016/j.ndteint.2014.02.005

Yang, K.; Nanukuttan, S. V.; McCarter, W. J.; Long, A.; and Basheer, P. A. M., 2018, "Challenges and Opportunities for Assessing Transport Properties of High-performance Concrete," *Revista ALCONPAT*, V. 8, No. 3, pp. 246-263. doi: 10.21041/ra.v8i3.301

Yang, L.; Liu, S.; Tsoka, S.; and Papageorgiou, L. G., 2016, "Mathematical Programming for Piecewise Linear Regression analysis," *Expert Systems with Applications*, V. 44, pp. 156-167. doi: 10.1016/j.eswa.2015.08.034

Yavuz, K., and Safak, E., 2019, "Structural Health Monitoring: Real-Time Data Analysis and Damage Detection," *Seismic Structural Health Monitoring*, M. P. Limongelli and M. Çelebi, eds., Springer, Cham, pp. 171-197.

Yu, C.; Wang, J.; Tan, L.; and Tu, X., 2011, "A Bridge Structural Health Data Analysis Model Based on Semi-supervised Learning," *IEEE International Conference on Automation and Logistics (ICAL)*, Chongqing, China, IEEE, pp. 30-34.

Zelić, J.; Rušić, D.; Veža, D.; and Krstulović, R., 2000, "Role of Silica Fume in the Kinetics and Mechanisms During the Early Stage of Cement Hydration," *Cement and Concrete Research*, V. 30, No. 10, pp. 1655-1662. doi: 10.1016/S0008-8846(00)00374-4

Zhang, C.; Zhang, W.; Webb, D. J.; and Peng, G. D., 2010, "Optical Fibre Temperature and Humidity Sensor," *Electronics Letters*, V. 46, No. 9, pp. 643-644. doi: 10.1049/el.2010.0879